


ORIGINAL RESEARCH

A DFT-based method for estimating interharmonics in wind power generation

Henrique L. M. Monteiro¹ | Ândrei Camponogara² | Moisés V. Ribeiro³  |
Carlos A. Duque³ | H. Vincent Poor⁴

¹Institute of Science, Technology and Innovation of São Sebastião do Paraíso, Federal University of Lavras, Lavras, Brazil

²Electrical Engineering Department, Federal University of Paraná, Curitiba, Brazil

³Department of Electrical Engineering, Federal University of Juiz de Fora, Juiz de Fora, Brazil

⁴Department of Electrical and Computer Engineering, Princeton University, Princeton, New Jersey, USA

Correspondence

Moisés V. Ribeiro, Department of Electrical Engineering, Federal University of Juiz de Fora, Juiz de Fora 36036-330, Brazil.
Email: mribeiro@engenharia.ufjf.br

Funding information

Conselho Nacional de Desenvolvimento Científico e Tecnológico, Grant/Award Number: 404068/2020-0; Fundação de Amparo à Pesquisa do Estado de Minas Gerais, Grant/Award Number: APQ-03609-17; Coordenação de Aperfeiçoamento de Pessoal de Nível Superior, Grant/Award Number: Finance Code 001; Instituto Nacional de Energia Elétrica

Abstract

This paper introduces a discrete Fourier transform (DFT)-based method for estimating the amplitudes and frequencies of interharmonics, which arise from the interaction between wind power generators and electric power systems. This method exploits the synergy of choosing signal enhancement, mains frequency estimation, and re-sampling techniques. Consequently, it accomplishes a cost-effective estimation process. The performance results show that signal enhancement and re-sampling techniques are necessary to establish suitable conditions for performing amplitude and frequency estimation. Furthermore, numerical results show that the proposed method, relying on low-cost digital signal processing techniques, offers competitive performance and significant computational complexity reduction compared to a previous DFT-based method.

KEYWORDS

discrete time systems, power supply quality, power system measurement, renewable energy sources, wind power plants

1 | INTRODUCTION

The increasing penetration of renewable energy sources based on wind power turbines has increased the concerns about the presence of interharmonics in electric signals. These interharmonics are specific disturbances in electric signals that result from the interaction between wind power generators and electric power systems [1–3]. Indeed, interharmonics are recognised as the underlying source of turbine shaft breaks, overheating, equipment degradation, voltage fluctuations, and light flicker [4–6]. Also, they can affect the stability and quality of electric power systems. Consequently, interharmonics monitoring constitutes an essential task to quantify the degradation inserted by interharmonics.

The International Electrotechnical Commission (IEC) 61000-4-7 standard, relying on the discrete Fourier transform

(DFT), describes a procedure to estimate the harmonic and interharmonic components by considering groups and sub-groups of tones [7]. For obtaining the frequency resolution of 5 Hz, the IEC 61000-4-7 standard specifies finite-length sequences that correspond to 12 and 10 cycles for 60 and 50 Hz mains frequencies, respectively. The highest harmonic considered in this standard is the 50th. Essentially, it groups the energy contained around each harmonic to estimate its magnitude, and the frequency assigned to an interharmonic is the mean value between two consecutive harmonics, which may not be a reasonable procedure for characterising interharmonics.

Recognising the necessity for improvements, several studies have introduced methods to estimate the parameters of interharmonics. Ref. [8] presented a method based on Vortex search, while Ref. [9] introduced the use of the Kalman filter (KF), which was further improved in Ref. [10]. Moreover, multiple

This is an open access article under the terms of the Creative Commons Attribution-NonCommercial-NoDerivs License, which permits use and distribution in any medium, provided the original work is properly cited, the use is non-commercial and no modifications or adaptations are made.

© 2022 The Authors. *IET Smart Grid* published by John Wiley & Sons Ltd on behalf of The Institution of Engineering and Technology.

signal classification, Prony's method, estimation based on rotational invariance technique (ESPRIT), adaptive linear element, matching pursuit, and discrete wavelet transform [11–16] were considered. The genetic algorithm [17], least-squares optimisation [18], machine learning [19], deep learning [20], and independent component analysis [21] methods were also considered. Some of the above-mentioned methods present good performance; however, it is attained by demanding high computational complexity.

Furthermore, there is a considerable interest in designing DFT-based methods to estimate the parameters of interharmonics in electric power systems. The reason for such attractiveness is the advantageous trade-off between performance and computational complexity since the DFT is already standardised to estimate parameters of harmonics. In other words, if we are capable of using the DFT to estimate the parameters of harmonics and interharmonics, then we can reduce the computational complexity associated with the estimation process. Nonetheless, the spectral leakage degrades the performance of DFT-based methods. Ref. [22] introduced the interpolated discrete Fourier transform (IpDFT), which aims to estimate the frequency of interharmonics, while Ref. [23] proposed a three-point IpDFT method to estimate the parameters of frequency components. Also, Ref. [24] introduced an enhanced IpDFT, which relies on the Hilbert transform to improve the estimation process. It is important to emphasise that the accuracy of the IpDFT is compromised under the presence of spectral leakage, which occurs when the monitored electric signal is not coherently sampled concerning harmonics. Consequently, it is necessary to investigate tools capable of mitigating spectral leakage.

To improve the performance of estimation methods applied to interharmonics, which are contaminated by the presence of non-coherently sampled harmonics, the combination of re-sampling and IpDFT is a valuable research direction. For instance, Ref. [25] uses pre-filters based on the inverse function of the cubic spline to perform re-sampling while Ref. [26] focusses on pre-filters designed via least-squares approximation with the same aim. Both methods result in more computational complexity since the performance of the designed pre-filters increases with their order. A comparison between re-sampling techniques proposed in Ref. [25, 26] was detailed in Ref. [27] in the context of the IEC 61000-4-7 standard. From the above discussion, the research direction for improving the parameter estimation process for interharmonics is to advance the combination of signal enhancement, re-sampling, and DFT-based methods.

This paper proposes a combination of signal enhancement, re-sampling, and amplitude and frequency estimation techniques that leads to improved performance and reduced computational complexity when a DFT-based method is taken into account. Signal enhancement creates a condition to facilitate the estimation process while re-sampling mitigates spectral leakage associated with harmonics when they are not

coherently sampled. Furthermore, the proposed DFT-based method exploits the fact that only one interharmonic exists between two consecutive harmonics. Consequently, a simple technique is applied to estimate the amplitude and frequency of interharmonics. In other words, this paper proposes an efficient, robust, and low computational complexity DFT-based method for estimating the parameters of interharmonics. Furthermore, the proposed method offers good accuracy in various scenarios such as frequency deviation and presence of noise, besides being a promising technique in practical applications. The main contributions are as follows:

- A discussion of the benefits related to the combination of a simple digital filter-based signal enhancement technique concatenated to the zero-crossing-based frequency estimation for providing low-cost and improved mains frequency estimates.
- A presentation of the simplicity of using the Lagrange interpolation with the Farrow structure for re-sampling electric signals and ensuring harmonics are always coherently sampled, which significantly improve the performance of the parameter estimation technique applied to interharmonics.
- A discussion of a simple technique to estimate the amplitude and frequency of a single interharmonic localised between two consecutive harmonics.

Based on the provided discussions and numerical results, we unveil the following findings:

- A suitable combination of low-pass and pass-band digital filters offers the necessary signal enhancement for allowing a low-cost mains frequency estimation technique to attain improved performance.
- The implementation of Lagrange interpolation with the Farrow structure is effective for re-sampling electric signals with the advantage of offering low computational complexity.
- The proposed method offers improved performance and significant computational complexity reduction in comparison to previous DFT-based methods.
- The gains attained with the appropriate combination of digital signal processing-based techniques, which are described in this contribution, result in an effective and efficient DFT-method for estimating the parameters of interharmonics in wind power generation plants or similar scenarios.

The rest of this paper is organised as follows: Section 2 formulates the investigated problem; Section 3 details the proposed DFT-based method; Section 4 focusses on signal enhancement and mains frequency estimation; Section 5 discusses re-sampling; Section 6 addresses amplitude and frequency estimations; Section 7 presents numerical results and performance comparisons; finally, Section 8 contains our concluding remarks.

2 | PROBLEM FORMULATION

Let us assume that an electric signal (i.e. voltage or current) can be modelled by the following random process [28–30]:

$$\begin{aligned}
 x(t) = & A_0 + \sum_{k=1}^{N_1} A_k \cos(k\Omega_0(t)t + \theta_k(t)) \\
 & + \sum_{l=1}^{N_2} A_{I,l} \cos(\Omega_{I,l}t + \theta_{I,l}(t)) \\
 & + \sum_{l=1}^{N_3} A_{S,l} \cos(\Omega_{S,l}t + \theta_{S,l}(t)) \\
 & + \sum_{l=1}^{N_4} x_{\text{imp},l}(t) + \sum_{l=1}^{N_5} x_{\text{not},l}(t) \\
 & + \sum_{l=1}^{N_6} x_{\text{osc},l}(t) + v(t),
 \end{aligned} \tag{1}$$

where $-\infty < t < +\infty$; A_0 is the direct current (DC) component; $\{A_1, \Omega_0(t), \theta_1(t)\}$, $\{A_k, k\Omega_0(t), \theta_k(t)\}$, $\{A_{I,l}, \Omega_{I,l}, \theta_{I,l}(t)\}$, and $\{A_{S,l}, \Omega_{S,l}, \theta_{S,l}(t)\}$ are the parameters of time-varying mains, harmonic, interharmonic, and supraharmonic components, respectively; $\Omega_0(t) = 2\pi f_0(t)$ and $f_0(t)$ is the time-varying mains frequency. Moreover, $x_{\text{imp},l}(t)$, $x_{\text{not},l}(t)$, and $x_{\text{osc},l}(t)$ denote the l th impulse, l th notch, and l th damped oscillatory transients, respectively, which are supposed to be random processes. Note that N_1 , N_2 , and N_3 are the number of mains plus harmonics, interharmonics, and supraharmonics, respectively, while N_4 , N_5 and N_6 refer to the number of the aforementioned transients. We assume that the additive noise, $v(t)$, and transient components are zero mean wide-sense stationary random processes. In addition, $v(t)$ is modelled as a Gaussian random process.

The link between the components in electric signals (i.e. waveform distortions in electric signals) and specific events is well established. A brief description of a few events that manifest in the form of waveform distortions in electric signals is as follows:

- DC: It is induced into the electric power system when a rectifier fails since alternating current/DC conversion can add unwanted current to devices already operating at their rated level. The circulation of DC currents can provoke overheating and saturation of transformers [31].
- Mains component: Distortions in this component refer to variations of its amplitude and frequency values [32, 33]. Amplitude variation can result in flickering lights, insulation degradation, data corruption, industrial processing errors, and other problems. Frequency variations make motors or sensitive devices inefficient.
- Harmonics: They are caused by the interaction between electric power systems and non-linear loads [34]. They can result in over-voltage, equipment malfunction, equipment heating, and damage, among other problems [35].
- Interharmonics: These components are characterised by frequencies that are non-integer multiple of the mains

frequency. Interharmonics are observed in the operation of static frequency converters, cycloconverters, subsynchronous converter cascades, adjustable speed drives for induction or synchronous motors, arc furnaces, and other loads that are not pulsating synchronously with the mains frequency [4]. They can cause overheating and reduced lifetime of equipment, sub-synchronous oscillations, voltage fluctuations, unintended tripping of protection circuits, and flickering lights, among other problems [36].

- Supraharmonics: These high-frequency distortions refer to waveform distortions related to the frequency range 2–150 kHz [37]. They can cause heating losses, audible noises, malfunction of equipment, flickering light, and undesirable tripping of the earth-leakage differential protection, among other problems [38].
- Impulsive transients: These refer to random and non-periodic, sudden, and high peak variations in the amplitude of electric signals. They can cause the loss (or corruption) of data and physical damage of equipment. Lightning is probably the most damaging type of impulsive transient.
- Oscillatory transients: They are random processes associated with sudden changes in the steady-state conditions of electric signals that manifest in the form of decaying oscillations [39, 40].
- Notch transients: These are modelled as cyclostationary random processes and are related to a typical disturbance in voltage signals. They can cause halts, data loss, and data transmission problems [41].
- Additive noise: This combines thermal noise and radio signals induced into unshielded power lines. It can result in equipment malfunction and long-term component failure, among other problems.

Concerning interharmonics, attention should be paid to these components in electric signals because they can cause serious problems, as mentioned above. Interharmonics are present mainly in electric power systems that rely on power electronics to interconnect electric power circuits operating with distinct frequencies (e.g. transmission electric power grid and wind power generation circuits). Regarding interharmonics in such interconnections, the following model applies [42]:

$$f_i = (p_1 m \pm 1)f_0 \pm f_r \tag{2}$$

in which f_i is the interharmonic frequency, $p_1 \in \mathbb{N} - \{0\}$ is the pulse number of the rectifier section, $m \in \mathbb{Z}$ is an integer, f_0 is the mains frequency, and f_r is the ripple frequency.

In wind power generation, the interharmonic frequencies are located between the DC and mains frequencies and between the mains frequency and the second harmonic [43]. Double-fed induction generators and series compensation-based transmission electric power systems, which are interconnected to the wind power generation circuit, are responsible for producing and injecting these undesirable components into electric signals.

Analyses of electric signals in the time, frequency, and spatial dimensions are essential to monitor and predict the dynamics of electric power systems. These tasks can be facilitated by performing synchronous digitisation of electric signals¹; however, characteristics of measuring units create difficulties for ensuring synchronous digitisation of electric signals. Moreover, the presence of distinct and undesirable components in electric signals imposes the necessity of applying complex and robust tools to analyse these signals. Therefore, the principle of *divide to conquer* has been widely considered in different applications.

Recently, the increasing inclusion of wind-based renewable energy sources in electric power systems has brought greater attention to interharmonics generated by devices whose switching frequencies are not synchronised with the mains frequency (e.g. wind turbines). The wind turbines heavily rely on semiconductor devices with non-synchronised switching frequency to the mains frequency. Consequently, it may cause adverse effects on existing electric power systems' assets and loads. Unfortunately, the analysis of interharmonics is not a simple task to be accomplished as these components are located close to the mains frequency and the second harmonic component. As a result, the estimation of their parameters needs to be carefully addressed.

In this regard, let us assume that a band-limited version of an electric signal given by (1) (i.e. $X(f) = \mathcal{F}\{x(t)\} | X(f) = 0 \forall |f| \geq B$, where $\mathcal{F}\{\cdot\}$ denotes the continuous-time Fourier transform and $B \in \mathbb{R}_+$) is digitised using the sampling period $T_s = 1/f_s$, in which $f_s = 2B$. After the digitisation process, the following expression is obtained in the discrete-time domain:

$$\begin{aligned} x[n] = x(t)|_{t=nT_s} &= A_0 + \sum_{k=1}^{N_1} A_k \cos(k\omega_0[n]n + \theta_k[n]) \\ &+ \sum_{l=1}^{N_2} A_{I,l} \cos(\omega_{I,l}n + \theta_{I,l}[n]) \\ &+ \sum_{l=1}^{N_3} A_{S,l} \cos(\omega_{S,l}n + \theta_{S,l}[n]) \\ &+ \sum_{l=1}^{N_4} x_{\text{imp},l}[n] + \sum_{l=1}^{N_5} x_{\text{not},l}[n] \\ &+ \sum_{l=1}^{N_6} x_{\text{osc},l}[n] + v[n]. \end{aligned} \quad (3)$$

Relying on the use of the DFT for estimating parameters of interharmonics, a N -length sequence, which is constituted by samples of a causal sequence $\{x[n]\} | 0 \leq n < +\infty$ is considered. In practice, an N -length window sequence $\{w[n]\}_{n=0}^{N-1}$ is applied to $\{x[n]\}$. As a result, we obtain the following finite-length sequence:

$$x_{w,l}[n] = x[n - lN]w[n], \quad 0 \leq l < \infty, \quad 0 \leq n \leq N - 1. \quad (4)$$

Discussion of the type of window sequence and the existence of overlaps between consecutive N -length sequences is beyond the scope of our work; however, based on Ref. [43], we adopt the Hanning window and non-overlap between consecutive N -length sequences. As well-established in the literature, the DFT is an appropriate technique to detect and estimate the parameters of interharmonics if $\Delta\omega = 2\pi/N$ or $\Delta\omega_e = 2\pi/M$, in which $M \in \mathbb{N} - \{0\}$ denotes the length of the zero-padded² version of $x_w[n]$ ³, ensures that the tones associated with interharmonics agree with the tones of a N - or M -length DFT, respectively. However, as the frequencies of interharmonics are not integer multiples of the mains frequency, the value of N or the choice of M may incur tremendous computational burden because the DFT's frequency resolution must correspond to a very short frequency resolution in the continuous-frequency domain (e.g. $0 < \Delta f \leq 5$ Hz). In other words, the sampling frequency must increase beyond what is feasible to obtain a large N value, or the value of M must be considerably high. Then, both approaches give rise to improved performance and significant computational complexity.

Moreover, we remind ourselves that electric signals can be submitted to synchronous/coherent or asynchronous/non-coherent sampling processes that are supposed to be related to harmonics. The former sampling process refers to f_s for ensuring the harmonics are synchronously acquired, while the latter assumes f_s , providing an asynchronous acquisition of electric signals. It is important to emphasise that DFT-based methods rely on the coherent sampling process since it guarantees that harmonics are located over the tones of the DFT. Needless to say that the non-coherent sampling process always applies to interharmonics.

Assuming coherent sampling process for harmonics, we can state that the use of the DFT in the sequence $\{x_w[n]\}$, with the eyes on interharmonics, results in spectral leakage because the interharmonics are not located over the tones of the DFT, leading to poor estimates of interharmonics' parameters. For illustration purposes, Figure 1a,b show, respectively, the magnitude of the DFT of the discrete-time version of the electric signals given by

$$x_1(t) = 0.1 \cos(2\pi 83.5t) \quad (5)$$

and

$$x_2(t) = 0.1 \cos(2\pi 86.5t), \quad (6)$$

when $T_s = 0.097 \times 10^{-3}$ s and $N = 2048$, which corresponds to 12 cycles of the mains signal with $f_0 = 60$ Hz. Note that only the magnitudes of the DFT samples surrounding the interharmonic are shown. Giving the choice of T_s and N , we see

¹In our paper, we are assuming that synchronous digitisation means that all acquisition devices make use of a universal clock (e.g. GPS clock) and the same sampling frequency.

²Zero-padding is a helpful tool to increase spectral resolution of the DFT when the length of a sequence is small.

³For the sake of simplicity, the index l is omitted.

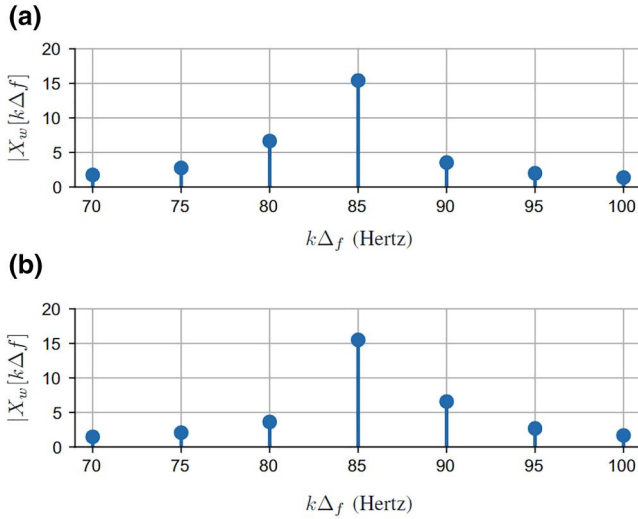


FIGURE 1 Spectral leakage around two interharmonic frequencies. (a) 83.5 Hz and (b) 86.5 Hz

that $\Delta\omega$ corresponds to $\Delta f = 5$ Hz. Note that the abscissa axis, in both graphs, is in terms of $k\Delta f$ because it facilitates the interpretation of the displayed waveforms.

According to Figure 1a,b, there is, as expected, a remarkable picket-fence effect and inspection of the frequency contents indicate that the interharmonic frequency is equal to 85 Hz, which is incorrect. Moreover, if we consider the frequency 85 Hz as an inflection point, we can see that the spectral leakage is higher on the left side when the interharmonic is located on the left side and vice-versa when the interharmonic is located on the right side. We can also observe similar results under the presence of harmonics, which we assume to be synchronously sampled, because the spectral leakage will be solely associated with interharmonics, which are asynchronously sampled.

As the devices used for monitoring wind power generators⁴ do not allow us ensure that harmonics be coherently sampled, the value of the mains frequency is not constant, and the presence of other components in electric signals degrades the performance of the DFT-based method applied to estimate interharmonics' parameters. Section 3 details a novel DFT method that is capable of minimising the aforementioned problems when we are dealing with interharmonics in wind power generation.

3 | ESTIMATING INTERHARMONICS

We noted in Section 2 clearly that a DFT-based method designed to estimate interharmonics' parameters in wind power generation has to guarantee high signal-to-noise ratio (SNR)

conditions and coherently sampled harmonics. High SNR can be accomplished via a signal enhancement technique, which needs to be carefully designed to reduce the power of disturbing components located outside the frequency band of interest. Note that we can ensure coherent sampling for harmonics as long as $f_0(t) = f_0$ Hz because sampling frequency is typically constant in data acquisition equipment. However, the dynamics of electric power systems impose that the mains frequency is time-varying (i.e. $f_0(t)$), and the sampling frequency may vary among the devices, meaning harmonics are asynchronously sampled. Therefore, it is necessary to apply a digital signal processing technique to re-sample the sequence $\{x_w[n]\}$ and to ensure harmonics are coherently sampled.

In this sense, let us assume that the sampled signal is given by Equation (3), the value of the mains frequency varies with time, the sampling frequency is $f_s = f_0 N_c$ with $f_0 \in \{50, 60\}$ Hz being the value the mains frequency⁵, $N = LN_c$ and $L, N_c \in \mathbb{N} - \{0\}$ are the numbers of cycles of the mains signal and the number of points in each cycle, respectively, and N is the length of a sequence that will be used to estimate the parameters of interharmonics in the discrete-frequency domain, which is provided by the DFT. In practice, it is necessary to estimate the mains frequency because the sampling process supposes that the mains frequency is equal to f_0 ; however, the correct value is $f'_0 = f_0(t)$, which is an estimate of $f_0(t)$ within a certain time interval covered by the N -length sequence $x_w[n]$ ⁶, and unfortunately, $f'_0 \neq f_0$.

Considering the model for electric signals and the necessity of estimating interharmonics' parameters in wind power generation, in which only one interharmonic is located in the frequency ranges defined by $[l f_0, (l + 1) f_0]$, $l \in \{0, 1\}$ (i.e. below f_0 Hz and between f_0 and $2f_0$ Hz), it is appealing to advance a DFT-based method for estimating parameters of interharmonics that incorporate the following enhancements:

- A suitable signal enhancement technique to remarkably reduce the influence of the spectral contents of distortions⁷ in the estimation process.
- A simple technique to estimate the mains frequency for performing re-sampling, which ensures harmonics are always coherently sampled⁸.
- A simple re-sampling technique to guarantee the harmonics are coherently sampled when the mains frequency is different from f_0 (e.g. 50 or 60 Hz).
- The use of a parameter estimation technique that can exploit the spectral leakage characteristic of the DFT when only interharmonics are supposed to be asynchronously sampled. It is critical because the interharmonics associated with wind power generation are around the mains frequency.

⁵The choice of this value depends upon the country. In Brazil, $f_0 = 60$ Hz.

⁶We assume that the coherence time for the mains frequency is longer than $T = NT_s$. In other words, $f_0(t) = f'_0$ in a time period of T seconds. Coherent time refers to a given time interval over which a given parameter presents negligible variation.

⁷For estimating the parameters of interharmonics, other components are considered distortions, and their minimisation improves SNR.

⁸It ensures that the spectral leakage related to non-coherently sampled harmonics is negligible.

⁴It is possible to design data acquisition devices that ensure harmonics are coherently sampled; however, it will result in a significant cost increase. To overcome this problem, we rely on digital signal processing [29, 30, 42, 44–47] because it can result in feasible and simple solutions.

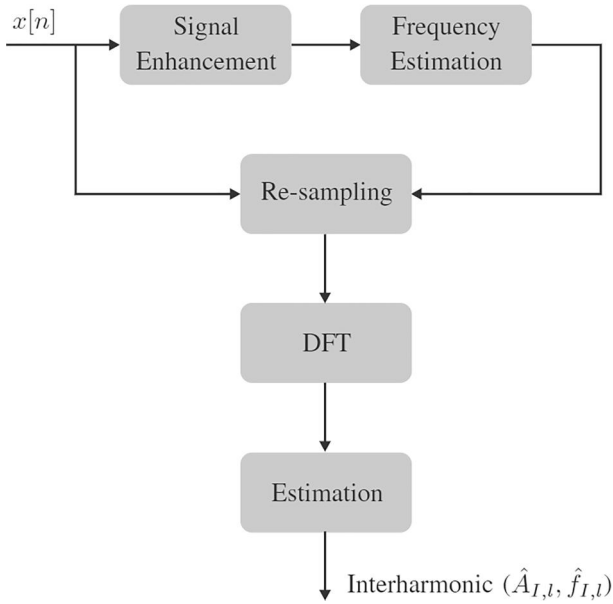


FIGURE 2 The block diagram of the proposed DFT-based method

Figure 2 shows a block diagram of the proposed DFT-based method that encompasses these enhancements. The first block represents the signal enhancement, the second block refers to mains frequency estimation, the third block deals with re-sampling, the fourth block refers to the DFT, and the fifth block represents the estimation of the parameters of interharmonics. To detail the proposed method, Section 4 focusses on signal enhancement and mains frequency estimation, while Section 5 addresses the use of re-sampling, and Section 6 addresses the estimation of parameters of interharmonics.

4 | DIGITAL FILTERING AND MAINS FREQUENCY ESTIMATION

The estimation of the mains frequency is essential in the proposed method because it drives the performance of the re-sampling process. The performance of a frequency estimation technique is degraded by the SNR associated with the mains signal, which is given by

$$\text{SNR}_{\text{mains}} = \frac{P_{\text{mains}}}{P_{\text{harm}} + P_{\text{inter}} + P_{\text{supra}} + P_{\text{imp}} + P_{\text{not}} + P_{\text{osc}} + P_v}, \quad (7)$$

where P_{mains} , P_{harm} , P_{inter} , P_{supra} , P_{imp} , P_{not} , P_{osc} , and P_v denote the powers associated with the mains, harmonics, interharmonics, supraharmatics, impulsive, notch, oscillatory, and additive noise components, respectively. To obtain a high SNR associated with the mains signal (e.g. $\text{SNR}_{\text{mains}} \rightarrow P_{\text{mains}}/P_{v,\text{mains}}$, where $P_{v,\text{mains}}$ refers to the power of the additive noise located over the mains frequency), it is necessary to apply a signal enhancement technique.

The design of a simple and effective signal enhancement technique based on digital filters [42] allows us to use a cost-effective technique to estimate the mains frequency. The designed signal enhancement technique is composed of the cascade of low-pass and band-pass infinite impulse response (IIR) digital filters. The former digital filter reduces the distortion inserted by high-frequency components, while the latter digital filter provides an additional signal enhancement around the mains frequency. This combination allows us to use digital filters that are very simple to design and demand a low computational burden.

The low-pass digital filter is a N_0 -order Butterworth IIR digital filter [44] designed with parameters (ω_p, N_0) ⁹, in which ω_p and N_0 refer to the band-pass frequency edge in 3-dB cutoff frequency and the filter order, respectively. The chosen band-pass IIR digital filter is of N_1 -order with ω_{mains} being the mains frequency in radian per sample, and B_ω is the frequency bandwidth, in radians, around ω_{mains} when the 3-dB cutoff frequency is considered [44].

Different techniques, such as the phase-locked loops, DFT, least-squares, KF, among others, can be used to estimate the mains frequency. However, we simplify the estimation process by using the zero-crossing technique [48] because the signal enhancement yielded by the digital filters remarkably reduces distortions in the waveform of electric signals that, in this case, are associated with the presence of different components from the mains frequency. The zero-crossing technique makes use of the last sample $x[n-1]$ in the previous (i.e. l th) mains cycle and the first sample $x[n]$ in the current ($l+1$ th) mains cycle to estimate the mains frequency, see illustration in Figure 3. The zero-crossing is a point over a linear function passing through both samples. It is obtained by solving the following system of equations:

$$\frac{x[n-1]}{K} = -\frac{x[n]}{P} \quad \text{and} \quad K + P = 1. \quad (8)$$

Manipulating Equation (8), we come up with the following values:

$$K = \frac{x[n-1]}{x[n-1] - x[n]}, \quad P = -\frac{x[n]}{x[n-1] - x[n]}, \quad (9)$$

where K and P correspond to the time intervals between the sample $x[n-1]$ and zero-crossing point and zero-crossing point and the sample $x[n]$, respectively. Finally, the estimated sampling period and mains period in the l th mains cycle is given by

$$\begin{aligned} T'_s[l] &= P[l]T_s \quad \text{and} \\ T'[l] &= T + T_s - T'_s[l], \end{aligned} \quad (10)$$

⁹The typical specification for designing such a filter is to define the band-pass and stopband frequency edges as well as the attenuation in the band-pass and stopband; however, we decided to use only the band-pass frequency edge and the filter order. This allows us to design the digital filter based on its order. It is another way of designing a low-order digital filter.

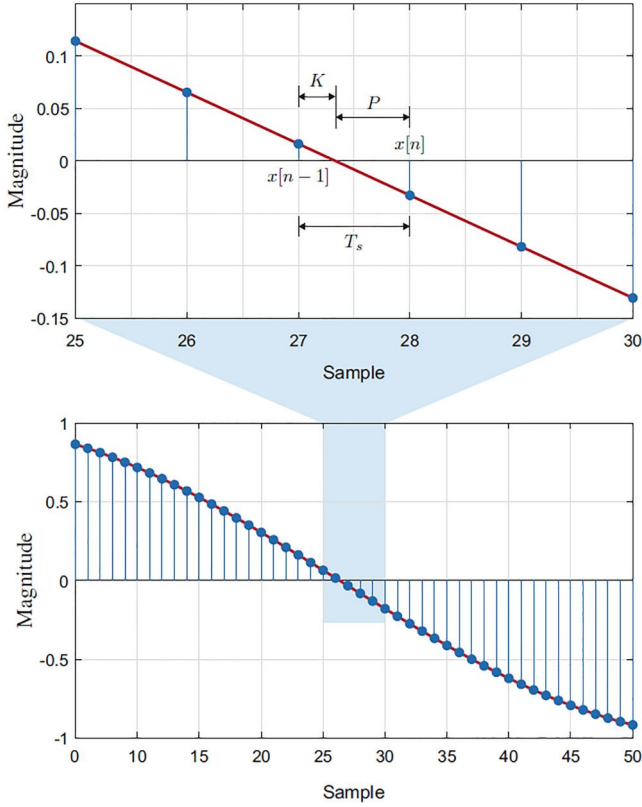


FIGURE 3 Details about zero-crossing associated with the mains frequency

respectively, in which T is the value of the mains period when the mains frequency is $f_0 \in \{50, 60\}$ Hz. As a result, the estimate of the mains frequency in the l th mains cycle is given by

$$f'_0[l] = \frac{1}{T'[l]}. \quad (11)$$

Aiming to smooth the residual distortions at the output of the signal enhancement technique, the estimate of the mains frequency is given by

$$f'_0 = \frac{1}{L} \sum_{l=0}^{L-1} f'_0[l], \quad (12)$$

where L is the number of estimates of the mains frequency.

5 | SEQUENCE RE-SAMPLING

Non-coherent sampling substantially degrades the performance of parameter estimation of interharmonics when the DFT is taken into account. Regarding wind power generation, we pointed out that coherently sampled harmonics result in spectral leakage related to interharmonics if the electric signal consists only of harmonics and interharmonics. This scenario can be obtained using a well-designed low-pass digital filter, concentrating on harmonics and interharmonics.

As the mains frequency may vary from its nominal value (i.e. 50 or 60 Hz), it is necessary to apply a technique to re-sample the acquired electric signals because it ensures harmonics are coherently sampled. The re-sampling process is not a simple task since the re-sampling ratio may not be an integer number. Consequently, the re-sampling process may be better performed by using interpolation techniques as suggested in Ref. [44]. Both Lagrange- and spline-based interpolation techniques can be applied as they benefit from an implementation based on the Farrow structure, easily implemented in a digital signal processor. Between them, we have chosen the former interpolation technique because it does not require pre-filtering as the latter does, see Ref. [25, 26] for more details.

According to Ref. [44], a Lagrange-based interpolated sequence is given by

$$\begin{aligned} y[n] &= x(nT_s + \alpha T_s) \\ &= \sum_{k=-N_1}^{N_2} P_k(\alpha) x[n+k], \end{aligned} \quad (13)$$

where $\alpha \in \mathbb{R} | 0 < \alpha < T_s$, and $P_k(\alpha)$ is the Lagrange polynomial given by

$$P_k(\alpha) = \prod_{\substack{l=-N_1 \\ l \neq k}}^{N_2} \frac{(\alpha - l)}{(k - l)} \quad (14)$$

with $-N_1 \leq k \leq N_2$ and $\alpha = \text{mod}(T_s, T'_s)$, which returns the rest of T'_s/T_s , and $T'_s = 1/(Nf'_0)$.

Assuming that a third-order Lagrange polynomial with $N_1 = 2$ and $N_2 = 1$ is used to interpolate the discrete-time signal, we come up with the following expression:

$$\begin{aligned} y[n] &= \alpha_k^3 \left(-\frac{1}{6} x[n-2] + \frac{1}{2} x[n-1] - \frac{1}{2} x[n] + \frac{1}{6} x[n+1] \right) \\ &\quad + \alpha_k^2 \left(\frac{1}{2} x[n-1] - x[n] + \frac{1}{2} x[n+1] \right) \\ &\quad + \alpha_k \left(-\frac{1}{6} x[n-2] - x[n-1] + \frac{1}{2} x[n] + \frac{1}{3} x[n+1] \right) \\ &\quad + x[n], \end{aligned} \quad (15)$$

where $\alpha_k = k\alpha$ when we assume $n = 0 + k$, $k = 0, 1, \dots, K$ with $K = \max\{k\}$ subject to $k\alpha < 1$. We increment k and calculate $\alpha_k = k\alpha$ as long as $k\alpha < 1$. If $k\alpha > 1$, then we start over the process to update α_k with $n = K + k$, $k = 0, 1, \dots, K$ and so on. Note that these digital filters perform the interpolation using samples $x[n-2]$ to $x[n+1]$ to re-sample the samples $x[n]$.

It is important to emphasise that Equation (15) is a difference equation of a non-causal time-varying system. Consequently, delay must be included in order to have a causal time-varying system. This time-varying system can be implemented

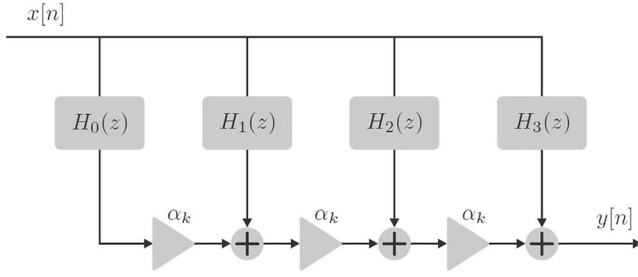


FIGURE 4 The Farrow structure for implementing a third-order Lagrange polynomial

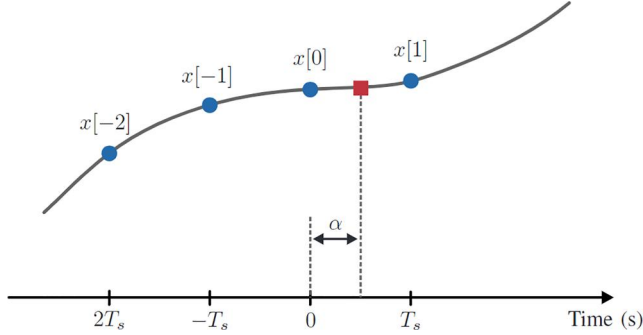


FIGURE 5 Illustration of the re-sampled point

using the Farrow structure shown in Figure 4, in which the transfer functions of finite impulse response (FIR) digital filters are given by

$$\begin{aligned} H_0(z) &= -\frac{1}{6}z^{-2} + \frac{1}{2}z^{-1} - \frac{1}{2} + \frac{1}{6}z \\ H_1(z) &= \frac{1}{2}z^{-1} - 1 + \frac{1}{2}z \\ H_2(z) &= \frac{1}{6}z^{-2} - z^{-1} + \frac{1}{2} + \frac{1}{3}z \\ H_3(z) &= 1. \end{aligned} \quad (16)$$

To illustrate the re-sampling process, Figure 5 shows the corresponding four samples over a continuous-time signal, which was non-coherently sampled. The re-sampled point in the interval between $x(nT_s) = x[n]$ and $x((n+1)T_s) = x[n+1]$. Moreover, to show how the re-sampling process works, Figure 6 shows the sequences with and without re-sampling. Both sequences are constituted of one sinusoidal component with the mains frequency equal to 58 Hz. Note that the re-sampled sequence has an integer number of cycles, whereas the sequence without re-sampling does not. The frequency spectrum of two signals, with and without re-sampling, is discussed in Section 7.

Ensuring harmonics are always coherently sampled, the spectral leakage around harmonics, in the discrete-frequency domain provided by the DFT, is solely related to interharmonics. Therefore, Section 6 emphasises the benefits of re-sampling for estimating the amplitude and frequency of interharmonics.

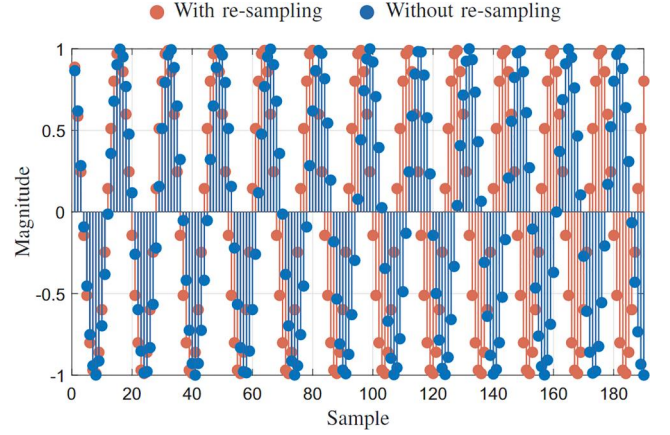


FIGURE 6 Sinusoidal signal with and without re-sampling

6 | INTERHARMONIC PARAMETER ESTIMATION

Relying on the benefits obtained by using the signal enhancement and re-sampling techniques, this section discusses a simple technique to estimate the amplitude and frequency of interharmonics.

Let $\{X_w[k]\}_{k=0}^{N-1}$ be the sequence obtained after applying the DFT in Equation (4), which is assumed to be corrupted solely by coherently sampled harmonics and non-coherently sampled interharmonics¹⁰. Coarse localisation of interharmonics determines the frequency range where the interharmonics are assumed to be located. To provide such coarse localisation, we first define the range index set denoted by $\mathcal{K}_\lambda = \{k \in \mathbb{N} \mid |X_w[k]| > \lambda \max |X_w[k]|\}$, where $0 < \lambda < 1$, which is illustrated in Figure 7. Next, we define two subsets of indices that are contained in the set \mathcal{K}_λ . The former subset is composed of the indices in \mathcal{K}_λ corresponding to the frequencies lower than f_0 and denoted \mathcal{K}_λ^- while the latter subset is composed of the indices related to frequencies higher than f_0 and lower than $2f_0$, which is denoted \mathcal{K}_λ^+ . The obtained sequences are denoted by $\{X^-[k]\} = \{X_w[k]\}_{\mathcal{K}_\lambda^-}$ and $\{X^+[k]\} = \{X_w[k]\}_{\mathcal{K}_\lambda^+}$. Now, we seek the indices related to the three highest magnitude values in $\{X^-[k]\}$ and $\{X^+[k]\}$. These indices are denoted by $\{k_0^-, k_1^-, k_2^-\}$ and $\{k_0^+, k_1^+, k_2^+\}$, which refer to the highest magnitude values below f_0 Hz and between f_0 and $2f_0$ Hz, respectively. As only one interharmonic can be observed in each frequency range [43], we can estimate the frequencies of interharmonics located below f_0 (i.e. \hat{f}_I^-) and between f_0 and $2f_0$, \hat{f}_I^+ , using

$$\hat{f}_I^- = (k_1^- + \delta^-) \frac{f_s}{N} \quad (17)$$

and

$$\hat{f}_I^+ = (k_1^+ + \delta^+) \frac{f_s}{N}, \quad (18)$$

¹⁰We are also assuming that distortions of high-frequency contents are filtered out by a signal enhancement technique (e.g. a low-pass digital filter).

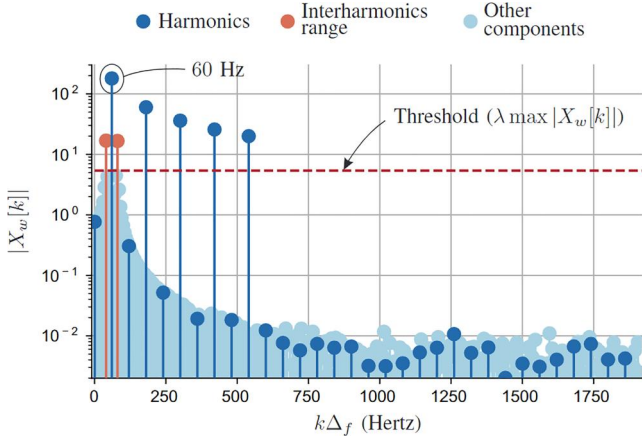


FIGURE 7 Threshold applied to an electric signal in the frequency domain to detect the interharmonic range

respectively, where δ^- and δ^+ are fractional compensations obtained by interpolating $\{X^-[k_0^-], X^-[k_1^-], X^-[k_2^-]\}$ and $\{X^+[k_0^+], X^+[k_1^+], X^+[k_2^+]\}$, respectively. Note that δ^- and δ^+ are given by

$$\delta^- = \frac{|X^-[k_0^-]| - |X^-[k_2^-]|}{|X^-[k_0^-]| + 2|X^-[k_1^-]| + |X^-[k_2^-]|} \quad (19)$$

and

$$\delta^+ = \frac{|X^+[k_0^+]| - |X^+[k_2^+]|}{|X^+[k_0^+]| + 2|X^+[k_1^+]| + |X^+[k_2^+]|}, \quad (20)$$

respectively. The estimates of the corresponding interharmonics are given by [43]

$$\hat{A}_I^- = |X^-[k_1^-]| \frac{\pi\delta^-}{\sin(\pi\delta^-)} [(\delta^-)^2 - 1] \quad (21)$$

and

$$\hat{A}_I^+ = |X^+[k_1^+]| \frac{\pi\delta^+}{\sin(\pi\delta^+)} [(\delta^+)^2 - 1], \quad (22)$$

respectively.

Last but not least, the discussed procedure to estimate the frequencies and amplitudes of interharmonics can be applied to other frequency ranges as far as the assumptions remain (i.e. electric signal corrupted solely by coherently sampled harmonics, non-coherently sampled interharmonics, and only one interharmonic in each frequency range).

7 | NUMERICAL RESULTS

This section discusses the numerical results related to the parameter estimation of interharmonics using the proposed DFT-based method. In this sense, we assume $f_s = N_c f_0$ Hz, $N_c = 16$, $N = 12N_c$, $f_0 \in \{59.9, 60\}$ Hz, and $L = 12N_c$, which

comply with the IEC 61000-4-7 standard. Also, we adopt a second-order Butterworth low-pass IIR digital filter designed with $\omega_p = 2\pi 150/f_s$ and $N_0 = 2$ and a 12th-order band-pass IIR digital filter designed with $\omega_{\text{mains}} = 2\pi 60/f_s$ and $B_w = 2\pi 10/f_s$ for performing the signal enhancement to facilitate the estimation process of the mains frequency. Furthermore, we consider $\lambda = 0.03$ and the SNR of the mains frequency related to the additive noise that is equal to 45 and 70 dB¹¹.

To numerically analyse each part of the proposed DFT-based method and detail the synergistic gains related to its components, this section is organised as follows: Subsection 7.1 discusses the improvements related to signal enhancement for performing mains frequency estimation; Subsection 7.2 deals with the enhancements related to re-sampling; Subsection 7.3 details the performance of the amplitude and frequency estimation technique; Subsection 7.4 discusses a performance comparison in terms of amplitude and frequency estimation with two other DFT-based methods; finally, Subsection 7.5 provides a comparison in terms of computational complexity with two other DFT-based methods.

7.1 | Signal enhancement and mains frequency estimation

This subsection analyses the performance improvement of the mains frequency estimation process when it consists of a signal enhancement technique, which is comprised of the concatenation of the low-pass and band-pass IIR digital filters. In this sense, let an electric signal be constituted by the mains component, interharmonics around the mains frequency, and the additive noise. This signal can be expressed as

$$x[n] = \cos(2\pi 59.9nT_s) + 0.1 \cos(2\pi 50nT_s) + 0.1 \cos(2\pi 70nT_s) + v[n], \quad (23)$$

in which $f_0 = 59.9$ Hz. For such electric signal, Figure 8 shows estimates of the mains frequency, $f'_0[l]$, with and without the use of the designed signal enhancement technique. Also, it shows the value of f'_0 , which is obtained using an N_c -order FIR average digital filter, see Equation (12), when $f'_0[l]$ is obtained by using the designed signal enhancement technique. These results emphasise that signal enhancement significantly mitigates the mains frequency oscillation caused by the presence of interharmonics, which results in better mains frequency estimates when we use the zero-crossing technique, which is a very simple technique to be implemented. The simulation shows that $f'_0 = 59.90$ Hz, which agrees with the value in Equation (23).

The benefit behind the use of a signal enhancement technique is even more significant when the electric signal is also composed of harmonics. To illustrate this, we consider an electric signal composed of the mains component, the 3rd

¹¹In other words, the powers associated with the other components are not taken into account to define the SNR of the analysed electric signals, which are used for performing numerical simulations. This choice allows us to keep compatibility with previous studies in which the SNR was defined in the same way.

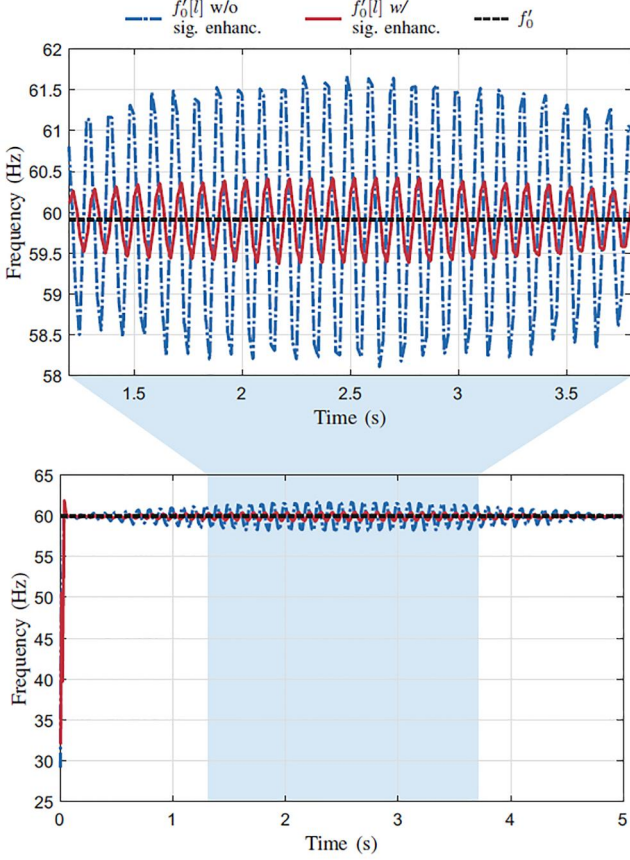


FIGURE 8 Estimates of mains frequency with the presence of interharmonics at frequencies 50 and 70 Hz

harmonic, whose magnitude is equal to 33.3% of the mains component, and interharmonics. This signal can be expressed as

$$x[n] = \cos(2\pi 59.9nT_s) + 0.1 \cos(2\pi 50nT_s) + 0.1 \cos(2\pi 70nT_s) + 0.333 \cos(2\pi 3 \times 59.9nT_s) + v[n]. \quad (24)$$

The mains frequency estimates $f'_0[l]$ with and without signal enhancement as well as the estimate f'_0 , which is obtained with the use of the signal enhancement technique, are shown in Figure 9. As we can see, signal enhancement reduces the distortions inserted by harmonics and interharmonics. Consequently, mains frequency estimation is improved and results in $f'_0 = 59.90$ Hz, which agrees with the value in Equation (24).

7.2 | Re-sampling results

To illustrate the usefulness of the re-sampling process, we assume that the electric signal is given by

$$x[n] = \cos(2\pi 59.4nT_s) + 0.1 \cos(2\pi 50nT_s) + 0.1 \cos(2\pi 70nT_s) + 0.2 \cos(2\pi 5 \times 59.9nT_s) + v[n], \quad (25)$$

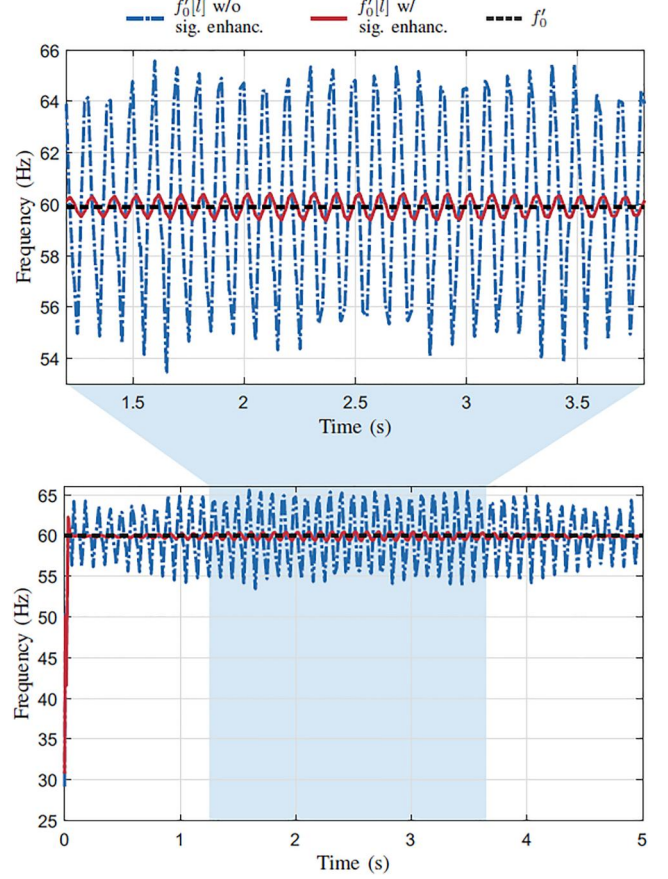


FIGURE 9 Estimates of mains frequency under the presence of the 5th harmonic and interharmonics at frequencies 50 and 70 Hz

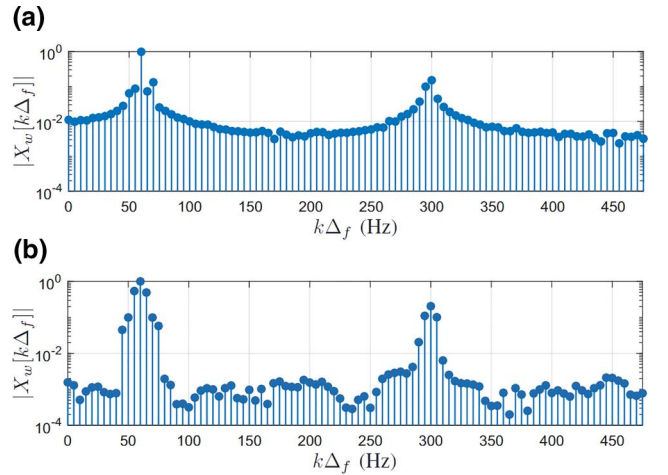


FIGURE 10 Spectrum of the mains signal under the presence of the 5th harmonic and interharmonics at frequencies 50 and 70 Hz. (a) Before re-sampling and (b) After re-sampling

in which we have the mains frequency, the 5th harmonic, two interharmonics, and the additive noise. Note that the harmonic's amplitude is 20% of the amplitude of the mains component.

Figure 10a,b show, respectively, the magnitudes of $X_w[k]$ of the electric signal before and after the re-sampling process when $\Delta_f = 5$ Hz. Observing these plots, we can see that

Figure 10a shows a spectral leakage because the harmonic is asynchronously sampled, whereas Figure 10b, in which the harmonics are synchronously sampled, shows spectral leakage only associated with interharmonics. In other words, the re-sampling process is effective to overcome the distortions inserted by asynchronously sampled harmonics.

7.3 | Interharmonic estimation

To show how the interharmonic estimation process performs, we consider the electric signal expressed as

$$x[n] = \cos(2\pi f_0 n T_s) + A_{I,1} \cos(2\pi f_{I,1} n T_s) + A_{I,2} \cos(2\pi f_{I,2} n T_s) + v[n], \quad (26)$$

where $A_{I,1} = 0.1$ and $A_{I,2} = 0.1$ are the interharmonics' amplitude with frequencies $f_{I,1} \in [10, 47]$ and $f_{I,2} \in [73-110]$, respectively, the SNR is equal to 45 dB and $f_0 \in \{59.9, 60\}$ Hz.

To assess the performance of the frequency estimation process for interharmonics, we consider the absolute error, which is given by

$$\Delta_{b_I, \text{error}} = |b_I - \hat{b}_I| \quad [\text{Hz}], \quad (27)$$

where $b_I \in \{f_{I,1}, f_{I,2}\}$ and \hat{b}_I are the true and the estimated values of the interharmonic's frequency, respectively. For performing the estimation process, we assume that the chosen values of $f_{I,1}$ and $f_{I,2}$ do not change within the L -length sequence obtained from Equation (26). To analyse the performance of the amplitude estimation process, we make use of the normalised absolute error, which is expressed as

$$a_{I, \text{error}} = 100 \frac{|a_I - \hat{a}_I|}{a_I} \quad [\%], \quad (28)$$

where $a_I \in \{A_{I,1}, A_{I,2}\}$ and \hat{a}_I are the true and the estimated values of the interharmonic's amplitude.

It is important to emphasise that this performance analysis assumes the use of the proposed DFT-based method in its totality. It is a necessary information because previous subsections analysed distinct parts of the proposed DFT-based method.

Figure 11a,b show $f_{I, \text{error}}$ in the frequency ranges 10–47 Hz and 73–110 Hz, respectively, and $f_0 = 60$ Hz. In these plots, we can see that $f_{I, \text{error}}$ values are lower than or equal to 65.20 and 94.30 mHz when the interharmonics are localised in the frequency ranges of 10–47 Hz and 73–110 Hz, respectively. Also, the values of $f_{I, \text{error}}$ are around 22.6 and 28.2 mHz, respectively, for these frequency ranges. Regarding the normalised absolute error, Figure 12a,b show $A_{I, \text{error}}$ for the frequency ranges of 10–47 Hz and 73–110 Hz, respectively. We can note that the maximum values of $A_{I, \text{error}}$ are around 1.26% and 1.49% for the interharmonics localised below and above $f_0 = 60$ Hz, respectively. Also, the values of $A_{I, \text{error}}$ obtained in these frequency ranges are 0.49% and 0.53%, respectively. Table 1 summarises some information about $f_{I, \text{error}}$ and $A_{I, \text{error}}$ for both frequency ranges.

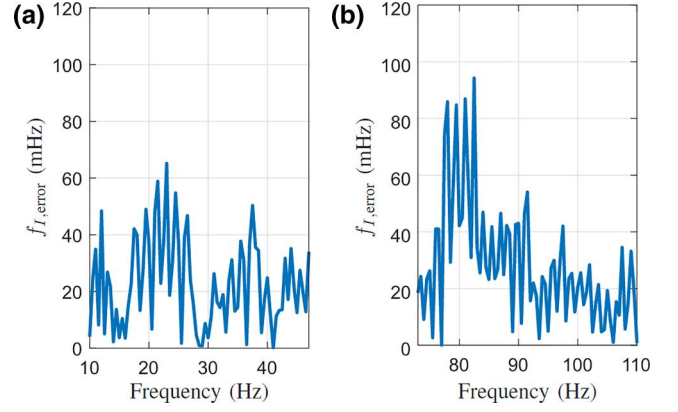


FIGURE 11 The values of the absolute error of the frequency estimates for the two frequency ranges when the mains frequency is without deviation (i.e. $f_0 = 60$ Hz). (a) 10–47 Hz and (b) 73–110 Hz

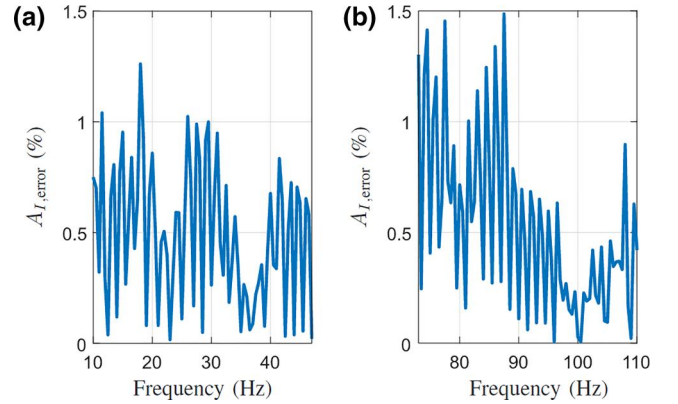


FIGURE 12 The values of the normalised absolute error of the amplitude estimates for the two frequency ranges when the mains frequency is without deviation (i.e. $f_0 = 60$ Hz). (a) 10–47 Hz and (b) 73–110 Hz

Figure 13a,b show $f_{I, \text{error}}$ for the frequency ranges 10–47 Hz and 73–110 Hz, respectively, and $f_0 = 59.9$ Hz. According to Figure 13, the maximum values of $f_{I, \text{error}}$ are equal to 64.0 and 108.3 mHz, respectively, for both frequency ranges when $f = 59.9$ Hz. Also, the mean values of $f_{I, \text{error}}$ around 20.4 and 30.2 mHz are found, respectively, for both frequency ranges. Additionally, Figure 14a,b show $A_{I, \text{error}}$ in terms of the frequency ranges 10–47 Hz and 73–110 Hz, respectively, considering a mains frequency of 59.90 Hz. In these figures, maximum values of $A_{I, \text{error}}$ equal to 1.18% and 1.31% are found for interharmonics localised in the frequency ranges 10–47 Hz and 73–110 Hz, respectively. Also, the maximum values of $A_{I, \text{error}}$ equal to 0.50% and 0.54% are observed, respectively, in these frequency ranges. Furthermore, Table 2 lists the maximum, mean, minimum, and standard deviation values of $f_{I, \text{error}}$ and $A_{I, \text{error}}$ for both frequency ranges.

Based on the reported results of $f_{I, \text{error}}$ and $A_{I, \text{error}}$, we can see that the proposed DFT-based method is effective to estimate the amplitude and frequency of interharmonics related to wind power generation. Indeed, the values of $f_{I, \text{error}}$ and $A_{I, \text{error}}$

Parameter	Frequency range (Hz)	Maximum	Mean	Minimum	Standard deviation
$f_{I,error}$	10–47	65.20 mHz	22.60 mHz	0.15 mHz	15.70 mHz
	73–110	94.30 mHz	28.20 mHz	0.02 mHz	21.10 mHz
$A_{I,error}$	10–47	1.26%	0.49%	0.01%	0.32%
	73–110	1.49%	0.53%	0.01%	0.39%

TABLE 1 Some information of $f_{I,error}$ and $A_{I,error}$ when $f_0 = 60$ Hz

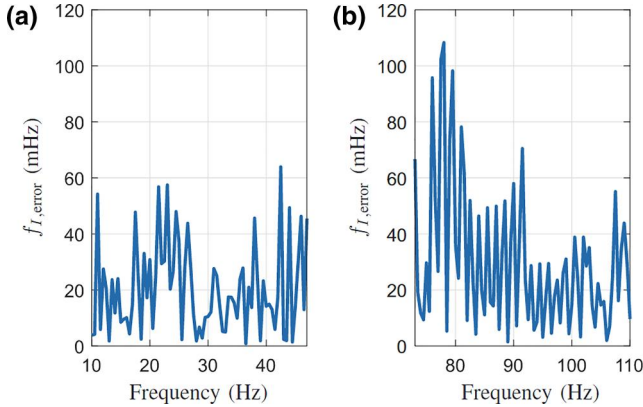


FIGURE 13 The values of the absolute error of the frequency estimates for the two frequency ranges when the mains frequency is with deviation (i.e. $f_0 = 59.9$ Hz). (a) 10–47 Hz and (b) 73–110 Hz

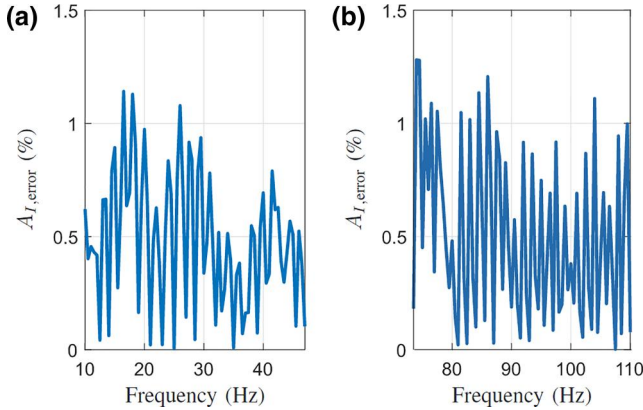


FIGURE 14 The values of the normalised absolute error of the amplitude estimates for the two frequency ranges when the mains frequency is with deviation (i.e. $f_0 = 59.9$ Hz). (a) 10–47 Hz and (b) 73–110 Hz

for the scenarios with and without a mains frequency deviation are fairly similar.

7.4 | Performance comparison

To carry out a performance comparison, we selected a partial version of the proposed DFT-based method, which is characterised by the absence of signal enhancement and re-sampling,

and a previous DFT-based method, which is detailed in Ref. [43]. The performance analysis of the partial version of the proposed DFT-based method aims to show the effectiveness of signal enhancement and re-sampling. In the following, we use terms Benchmark I and Benchmark II to denote, respectively, the partial version of the proposed DFT-based method and the method addressed in Ref. [43]. Also, we assume the electric signal given by Equation (26) presents a SNR equal to 70 dB, which agrees with Ref. [43], and interharmonics magnitudes ($A_{I,1}$ and $A_{I,2}$) varying in the range between 5% and 150% of the mains amplitude.

Table 3 summarises the absolute values for the frequency estimation error $f_{I,error}$ and the normalised absolute values for the amplitude estimation error $A_{I,error}$ when both frequency ranges are considered (i.e. below and above 60 Hz) and $f_0 = 59.93$ Hz for the proposed DFT-based and Benchmark I methods, and $f_0 = 49.93$ Hz for Benchmark II. The first difference between the proposed DFT-based, Benchmark I, and Benchmark II methods is related to the intended frequency ranges. The proposed DFT-based and Benchmark I method on 10–47 Hz and 73–110 Hz for the mains frequency equal to 59.93 Hz, while the Benchmark II considers 10–40 Hz and 60–90 Hz, which agree with Ref. [43] for the mains frequency equal to 49.93 Hz. According to Table 3, Benchmark II shows results slightly better than the proposed DFT-based method; however, the accuracy of the attained estimates is high, which makes such very small difference negligible. Moreover, Benchmark I attains the worst performance. Indeed, it attains absolute error for the frequency estimates of 18.47 Hz and 18.40 Hz for the interharmonics located in the frequency ranges of 10–47 Hz and 73–110 Hz, respectively, while the normalised absolute error for the amplitude estimates is equal to 1.59% for both frequency ranges. Note that the absence of signal enhancement, mains frequency estimation, and re-sampling techniques impose a severe degradation in Benchmark I when the mains frequency is different from 60 Hz.

7.5 | Computational complexity comparison

To carry out this comparison, Table 4 summarises the computational complexity of the proposed DFT-based method for performing signal enhancement, mains frequency estimation, re-sampling, DFT, and interharmonic's parameter estimation. Note that the computational complexity associated with the Benchmark I refers to the last two rows in Table 4. It is clear that the proposed DFT-based method is more complex than the Benchmark I.

TABLE 2 Some information of $f_{I,error}$ and $A_{I,error}$ when $f_0 = 59.9$ Hz

Estimation error	Frequency range (Hz)	Maximum	Mean	Minimum	Standard deviation
$f_{I,error}$	10–47	64.00 mHz	20.40 mHz	0.81 mHz	15.90 mHz
	73–110	108.30 mHz	30.20 mHz	1.50 mHz	25.40 mHz
$A_{I,error}$	10–47	1.18%	0.50%	0.01%	0.30%
	73–110	1.31%	0.54%	0.003%	0.39%

TABLE 3 Performance comparison: Proposed DFT-based, Benchmark I, and Benchmark II [43] methods

Proposed DFT-based method			Benchmark I			Benchmark II [43]		
Frequency range (Hz)	$f_{I,error}$ (mHz)	$A_{I,error}$ (%)	Frequency range (Hz)	$f_{I,error}$ (Hz)	$A_{I,error}$ (%)	Frequency range (Hz)	$f_{I,error}$ (mHz)	$A_{I,error}$ (%)
10–47	16.00	0.64	10–47	18.47	1.59	10 – 40	12.00	0.21
73–110	11.00	0.14	73–110	18.40	1.59	60 – 90	7.70	0.15

Abbreviation: DFT, discrete Fourier transform.

TABLE 4 Computational complexity of the proposed DFT-based method

Step	Operation	
	\times/\div	$+/-$
Signal Enhancement	$22N$	$41N$
Frequency Estimation	$20N + 104$	$21N + 66$
Re-sampling	$15N$	$11N$
DFT	$2N\log_2N$	$3N\log_2N$
Estimation process	15	6

Abbreviation: DFT, discrete Fourier transform.

TABLE 5 Computational complexity comparison: proposed DFT-based, Benchmark I and Benchmark II [43] methods

Method	Total of operations	
	\times/\div	$+/-$
Proposed DFT-based	13,976	18,457
Benchmark I	2927	4374
Benchmark II	1,255,450	2,682,112

Abbreviation: DFT, discrete Fourier transform.

The computational complexity comparison between the proposed DFT-based, Benchmark I, and Benchmark II methods are listed in Table 5. According to this table, the proposed DFT-based method demands a total number of multiplications/divisions equal to 13,976 and a total number of additions/subtractions equal to 18,457. In contrast, Benchmark II requires a total number of multiplications/divisions equal to 1,255,450 and a total number of additions/subtractions equal to 2,682,112. Moreover, Benchmark I attains 2927 multiplications/divisions and 4374 additions/subtractions. In other words, the proposed DFT-based method attains a remarkable computational complexity savings in

comparison to Benchmark II, which is detailed in Ref. [43], and more computational complexity than Benchmark I, which is a partial version of the proposed DFT-based method.

8 | CONCLUSION

This work has introduced a new DFT-based method to estimate amplitude and frequency of interharmonics, which result from wind power generation. The proposed DFT-based method takes advantage of improvements associated with signal enhancement to apply an effortless mains frequency estimation technique. Also, it takes advantage of a low-cost re-sampling technique to ensure that harmonics are always coherently sampled. Finally, it applies a simple interpolation in the frequency domain to estimate the amplitude and frequency of an interharmonic, which is assumed to be the only one occupying the frequency bands defined by the intervals $[0, f_0]$ and $[f_0, 2f_0]$.

Numerical results have shown that the proposed DFT-based method offers robust estimates of the mains frequency under the presence of typical disturbances in electric signals (e.g. harmonics and interharmonics) since signal enhancement is well designed. Also, these results show that re-sampling ensures the spectral leakage is only associated with interharmonics, which significantly improves the performance of amplitude and frequency estimation processes applied to interharmonics. Moreover, comparisons in terms of performance and computational complexity with two benchmark methods have shown that the proposed DFT-based method attains the best compromise between computational complexity reduction and performance improvement when the mains frequency is different from 50 Hz or 60 Hz.

As a final comment, we emphasise the existence of room for designing effective and efficient methods for analysing electric signals when careful design, combination, and adjustment of existing techniques are carried out to maximise synergy among them.

ACKNOWLEDGEMENTS

The authors would like to thank Coordenação de Aperfeiçoamento de Pessoal de Nível Superior (CAPES)-Finance Code 001, Fundação de Amparo à Pesquisa do Estado de Minas Gerais (FAPEMIG) - APQ-03609-17, Conselho Nacional de Desenvolvimento Científico e Tecnológico (CNPq)-404068/2020-0, and Instituto Nacional de Energia Elétrica (INERGE).

CONFLICT OF INTEREST

The authors declare no potential conflict of interest.

PERMISSION TO REPRODUCE MATERIALS FROM OTHER SOURCES

The authors permit the reproduction of all materials from other sources.

DATA AVAILABILITY STATEMENT

Data available on request.

ORCID

Moisés V. Ribeiro  <https://orcid.org/0000-0002-6272-4675>

REFERENCES

- Ravindran, V., Rönnberg, S.K., Bollen, M.H.: Interharmonics in PV systems: a review of analysis and estimation methods; considerations for selection of an apt method. *IET Renew. Power Gener.* 13(12), 2023–2032 (2019). <https://doi.org/10.1049/iet-rpg.2018.5697>
- Xie, X., et al.: Characteristic analysis of subsynchronous resonance in practical wind farms connected to series-compensated transmissions. *IEEE Trans. Energy Convers.* 32(3), 1117–1126 (2017). <https://doi.org/10.1109/tec.2017.2676024>
- Lin, H.C.: Development of interharmonics identification using enhanced-fft algorithm. *J. Eng.* 7, 333–342 (2017). <https://doi.org/10.1049/joe.2017.0133>
- Testa, A., et al.: Interharmonics: theory and modeling. *IEEE Trans. Power Deliv.* 22(4), 2335–2348 (2007). <https://doi.org/10.1109/tpwr.2007.905505>
- Zhang, P., et al.: An online measurement approach of generators' torsional mechanical damping coefficients for subsynchronous oscillation analysis. *IEEE Trans. Power Syst.* 30(2), 585–592 (2014)
- Lin, H.C.: Identification of interharmonics using disperse energy distribution algorithm for flicker troubleshooting. *IET Sci. Technol.* 10(7), 786–794 (2016). <https://doi.org/10.1049/iet-smt.2016.0110>
- Dalali, M., Jalilian, A.: Indices for measurement of harmonic distortion in power systems according to iec 61000-4-7 standard. *IET Gener., Transm. Distrib.* 9(14), 1903–1912 (2015). <https://doi.org/10.1049/iet-gtd.2015.0366>
- Altintasi, C., et al.: Power system harmonic and interharmonic estimation using vortex search algorithm. *Elec. Power Syst. Res.* 182, 106187 (2020). <https://doi.org/10.1016/j.epsr.2019.106187>
- Chen, C., et al.: Extended real model of kalman filter for time-varying harmonics estimation. *IEEE Trans. Power Deliv.* 25(1), 17–26 (2009). <https://doi.org/10.1109/tpwr.2009.2035217>
- Dhineshkumar, K., Subramani, C.: Kalman filter algorithm for mitigation of power system harmonics. *Int. J. Electr. Comput. Eng.* 8(2), 771 (2018). <https://doi.org/10.11591/ijece.v8i2.pp771-779>
- Cai, T., et al.: Real-valued music algorithm for power harmonics and interharmonics estimation. *Int. J. Circ. Theor. Appl.* 39(10), 1023–1035 (2011). <https://doi.org/10.1002/cta.684>
- Yalcin, N.A., Vatanserver, F.: A new hybrid method for signal estimation based on haar transform and prony analysis. *IEEE Trans. Instrum. Meas.* 70, 1–9 (2020). <https://doi.org/10.1109/tim.2020.3024358>
- Santos, E., et al.: Esprit associated with filter bank for power-line harmonics, sub-harmonics and inter-harmonics parameters estimation. *Int. J. Electr. Power Energy Syst.* 118, 105731 (2020). <https://doi.org/10.1016/j.ijepes.2019.105731>
- Chang, G.W., Chen, C.-I., Liang, Q.-W.: A two-stage adaline for harmonics and interharmonics measurement. *IEEE Trans. Ind. Electron.* 56(6), 2220–2228 (2009). <https://doi.org/10.1109/tie.2009.2017093>
- Li, Y., et al.: Detection of interharmonics using sparse signal decomposition based on ica-mp. *IEEE Trans. Instrum. Meas.* 70, 1–9 (2021). <https://doi.org/10.1109/tim.2021.3122185>
- Sezgin, E., Salor, O.: Analysis of power system harmonic subgroups of the electric arc furnace currents based on a hybrid time-frequency analysis method. *IEEE Trans. Ind. Appl.* 55(4), 4398–4406 (2019). <https://doi.org/10.1109/tia.2019.2911568>
- Bettayeb, M., Qidwai, U.: A hybrid least squares-ga-based algorithm for harmonic estimation. *IEEE Trans. Power Deliv.* 18(2), 377–382 (2003). <https://doi.org/10.1109/tpwr.2002.807458>
- He, S., et al.: A particle swarm optimizer with passive congregation. *Biosystems* 78(1-3), 135–147 (2004). <https://doi.org/10.1016/j.biosystems.2004.08.003>
- Garanayak, P., Naayagi, R., Panda, G.: A high-speed master-slave adaline for accurate power system harmonic and inter-harmonic estimation. *IEEE Access.* 8, 519181–51932, (2020). <https://doi.org/10.1109/access.2020.2980115>
- Balouji, E., et al.: Deep-learning-based harmonics and interharmonics predetection designed for compensating significantly time-varying eaf currents. *IEEE Trans. Ind. Appl.* 56(3), 3250–3260 (2020). <https://doi.org/10.1109/tia.2020.2976722>
- de Oliveira, D.R., et al.: Second order blind identification algorithm with exact model order estimation for harmonic and interharmonic decomposition with reduced complexity. *Int. J. Electr. Power Energy Syst.* 125, 106415 (2021). <https://doi.org/10.1016/j.ijepes.2020.106415>
- Derviškić, A., Romano, P., Paolone, M.: Iterative-interpolated DFT for synchrophasor estimation: a single algorithm for P-and M-class compliant PMUs. *IEEE Trans. Instrum. Meas.* 67(3), 547–558 (2017). <https://doi.org/10.1109/tim.2017.2779378>
- Chen, L., et al.: An interharmonic phasor and frequency estimator for subsynchronous oscillation identification and monitoring. *IEEE Trans. Instrum. Meas.* 68(6), 1714–1723 (2018). <https://doi.org/10.1109/tim.2018.2879998>
- Friego, G., Derviškić, A., Paolone, M.: Reduced leakage synchrophasor estimation: Hilbert transform plus interpolated DFT. *IEEE Trans. Instrum. Meas.* 68(10), 3468–3483 (2018). <https://doi.org/10.1109/tim.2018.2879070>
- Borkowski, D., Bien, A.: Improvement of accuracy of power system spectral analysis by coherent resampling. *IEEE Trans. Power Deliv.* 24(3), 1004–1013 (2009). <https://doi.org/10.1109/tpwr.2009.2013662>
- Petrinovic, D.: Causal cubic splines: formulations, interpolation properties and implementations. *IEEE Trans. Signal Process.* 56(11), 5442–5453 (2008). <https://doi.org/10.1109/tsp.2008.929133>
- Monteiro, H.L.M., et al.: Comparison of interpolation methods in time and frequency domain for the estimation of harmonics and interharmonics according to IEC standard. In: 16th IEEE International Conference on Harmonics and Quality of Power, pp. 1–5 (2014)
- Ribeiro, M.V., et al.: Benefits of energy recovery from the undesirable components of electric signals in electric power systems. *Int. J. Electr. Power Energy Syst.* 138, 107323 (2022). <https://doi.org/10.1016/j.ijepes.2021.107323>
- Ribeiro, M.V., et al.: Detection of disturbances in voltage signals for power quality analysis using hos. *Eurasip J. Adv. Signal Process.* 1, 059786 (2007). <https://doi.org/10.1155/2007/59786>
- Ribeiro, M.V., Pereira, J.L.R.: Classification of single and multiple disturbances in electric signals. *Eurasip J. Adv. Signal Process.* 1, 056918 (2007). <https://doi.org/10.1155/2007/56918>
- Buticchi, G., Consolini, L., Lorenzani, E.: Active filter for the removal of the dc current component for single-phase power lines. *IEEE Trans. Ind. Electron.* 60(10), 4403–4414 (2012). <https://doi.org/10.1109/tie.2012.2213562>

32. Köse, N., Salor, Ö., Leblebicioğlu, K.: Interharmonics analysis of power signals with fundamental frequency deviation using kalman filtering. *Elec. Power Syst. Res.* 80(9), 1145–1153 (2010). <https://doi.org/10.1016/j.epsr.2010.03.006>
33. Srinivasan, K.: Digital measurement of voltage flicker. *IEEE Trans. Power Deliv.* 6(4), 1593–1598 (1991). <https://doi.org/10.1109/61.97697>
34. Karafotis, P.A., Evangelopoulos, V.A., Georgilakis, P.S.: Evaluation of harmonic contribution to unbalance in power systems under non-stationary conditions using wavelet packet transform. *Elec. Power Syst. Res.* 178, 106026 (2020). <https://doi.org/10.1016/j.epsr.2019.106026>
35. Lin, H.C.: Power harmonics and interharmonics measurement using recursive group-harmonic power minimizing algorithm. *IEEE Trans. Ind. Electron.* 59(2), 1184–1193 (2012). <https://doi.org/10.1109/tie.2011.2157281>
36. Ravindran, V., et al.: Time-varying interharmonics in different types of grid-tied pv inverter systems. *IEEE Trans. Power Deliv.* 35(2), 483–496 (2020). <https://doi.org/10.1109/tpwrd.2019.2906995>
37. Grevener, A., et al.: Survey of supraharmonic emission of household appliances. *CIREC - Open Access Proc. J.* 1, 870–874 (2017). <https://doi.org/10.1049/oap-cired.2017.0458>
38. Espín-Delgado, Á., et al.: Summation law for supraharmonic currents (2–150 khz) in low-voltage installations. *Elec. Power Syst. Res.* 184, 106325 (2020). <https://doi.org/10.1016/j.epsr.2020.106325>
39. Hoffmann, A.B., et al.: Techniques for the diagnosis of oscillatory transients resulting from capacitor bank switching in medium voltage distribution systems. *Int. J. Electr. Power Energy Syst.* 133, 107198 (2021). <https://doi.org/10.1016/j.ijepes.2021.107198>
40. Bollen, M.H., Styvaktakis, E., Gu, I.Y.-H.: Categorization and analysis of power system transients. *IEEE Trans. Power Deliv.* 20(3), 2298–2306 (2005). <https://doi.org/10.1109/tpwrd.2004.843386>
41. Ghandehari, R., Shoulaie, A.: Evaluating voltage notch problems arising from ac/dc converter operation. *IEEE Trans. Power Electron.* 24(9), 2111–2119 (2009). <https://doi.org/10.1109/tpel.2009.2021058>
42. Ribeiro, P.F., et al.: *Power Systems Signal Processing for Smart Grids*. John Wiley & Sons (2013)
43. Chen, L., et al.: An interharmonic phasor and frequency estimator for subsynchronous oscillation identification and monitoring. *IEEE Trans. Instrum. Meas.* 68(6), 1714–1723 (2018). <https://doi.org/10.1109/tim.2018.2879998>
44. Mitra, S.K., Kuo, Y.: *Digital Signal Processing: A Computer-based Approach*. McGraw-Hill New York. 2 (2006)
45. Bollen, M.H., et al.: Bridging the gap between signal and power. *IEEE Signal Process. Mag.* 26(4), 12–31 (2009). <https://doi.org/10.1109/msp.2009.932706>
46. Tcheou, M.P., et al.: The compression of electric signal waveforms for smart grids: state of the art and future trends. *IEEE Trans. Smart Grid* 5(1), 291–302 (2014). <https://doi.org/10.1109/tsg.2013.2293957>
47. de Carvalho, J.R., et al.: A PLL-based multirate structure for time-varying power systems harmonic/interharmonic estimation. *IEEE Trans. Power Deliv.* 24(4), 1789–1800 (2009). <https://doi.org/10.1109/tpwrd.2009.2027474>
48. Sreenivas, T.V., Niederjohn, R.J.: Zero-crossing based spectral analysis and SVD spectral analysis for formant frequency estimation in noise. *IEEE Trans. Signal Process.* 40(2), 282–293 (1992). <https://doi.org/10.1109/78.124939>

How to cite this article: Monteiro, H.L.M., et al.: A DFT-based method for estimating interharmonics in wind power generation. *IET Smart Grid*. 1–15 (2022). <https://doi.org/10.1049/stg2.12072>